ACS Sustainable Chemistry & Engineering

Research Article

Cite This: ACS Sustainable Chem. Eng. 2018, 6, 2047−2054

Degradable Three Dimensional-Printed Polylactic Acid Scaffold with Long-Term Antibacterial Activity

Xiaoyuan Li,[†,‡] Yu Wang,[§] Min Guo,[§] Zongliang Wang,[§] Nannan Shao,[†,‡] Peibiao Zhang,[*,§] Xuesi Chen,[§] and Yubin Huang[*,†]

[†]State Key Laboratory of Polymer Physics and Chemistry and [§]Key Laboratory of Polymer Ecomaterials, Changchun Institute of Applied Chemistry, Chinese Academy of Sciences, No. 5625 Renmin Street, Changchun 130022, P. R. China

[‡]University of Chinese Academy of Sciences, No. 19(A) Yuquan Road, Beijing 100049, P. R. China

ABSTRACT: Polylactic acid (PLA) is one of the most promising candidates to solve the present environmental and energy problems. The programmable three-dimensional (3D) fabrication technique also provides a convenient and green platform for PLA applications in bone tissue engineering. An innovative PLA scaffold that combined multiple functions including highly interconnected porosity, sufficient nutrient supply, and antibacterial activity was prepared through 3D printing. Porosity of the scaffold was 67%, which was quite desirable for cell adherence and immigration. Followed by dopamine polymerization on the surface of the substrate, grafting with gelatin/nanohydroxyapatite (nHA) and ponericin G1 was further conducted. Scanning electron microscopy (SEM) and X-ray photoelectron spectroscopy (XPS) confirmed the successful modification. MC3T3-E1 cell culture showed a uniform distribution all through the scaffold with high survival rate, which was also confirmed by live/dead staining. Polydopamine modification made the scaffold totally hydrophilic and caused an early increase in cell proliferation, but the gelatin-containing group began to take effect at the later alkaline phosphatase (ALP) secretion stage. Scaffolds that were modified with ponericin (S/D/G/nHA/P group) improved calcium deposition to a large extent, as confirmed by alizarin red-S (ARS) staining. Both Gram-positive and -negative bacteria (*E. coli* and *S. aureus*) were effectively inhibited up to 24 h, and the inhibition zone could remain for 72 h. The comprehensive results showed that a balance was achieved between promoting the adhesion of MC3T3-E1 cells and simultaneous inhibition of pathogenic microbes.

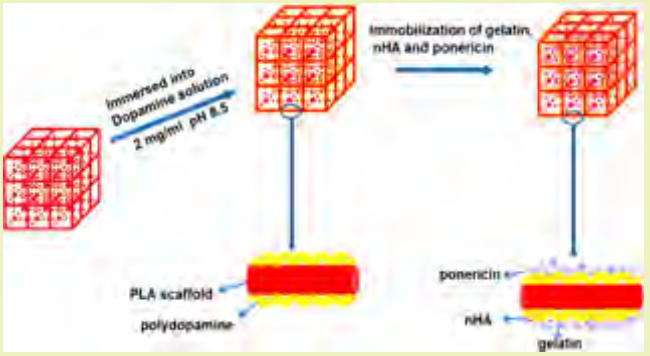

KEYWORDS: *3D-printed PLA, Ponericin G1, Dopamine, Antibacterial activity, Bone tissue engineering*

INTRODUCTION

The normal function of bone can be impaired by many traumatic injuries and some pathological disorders or congenital abnormalities. These malfunctions usually cause nonunion bone fractures, bone deformation, severe pain, and loss of mobility.[1,2] Although bone autografts are considered as the gold standard of treatment, their transplantation is limited because of additional infection, pain, and second-site morbidity.[3] For these problems to be addressed, tissue engineering has sparked and aimed to create a three-dimensional (3D) biocompatible support that can be inserted into a tissue to repair a lesion or correct a defect by allowing the adhesion and proliferation of a specific cell type.[4,5] Ideal bone graft substitutes should be able to comprehensively address the requirements for bone regeneration, such as the tunable ability to fill the space of the defect, sufficient interconnected pores to allow nutrient supply, good biocompatibility, and biodegradable properties. Although many conventional approaches could be applied for porous scaffold fabrication, such as gas foaming, solvent casting, particulate leaching, and electrospinning, 3D printing is becoming a more and more important technique in production processes for bone regeneration because it enables the fabrication of complex, multiscale structures through computer-aided design (CAD).[6−10] The term 3D printing, originally used to describe the process by which a binder material is deposited onto a powder bed with inkjet print heads, has evolved to be synonymous with additive manufacturing, which encompasses binder jetting, directed energy deposition, material extrusion, material jetting, powder bed fusion, sheet lamination, and vat photopolymerization technologies.[11]

On the basis of the material extrusion mechanism, fused deposition modeling (FDM) is often used to extrude a semiliquid paste that contains a molten thermoplastic polymer and to deposit the material by a computer-controlled extrusion system.[12] Conventional biodegradable PLA has been widely used for 3D printing,[13] but the absence of abundant functional groups makes a direct chemical modification difficult and

Received: September 27, 2017
Revised: November 30, 2017
Published: December 12, 2017

DOI: 10.1021/acssuschemeng.7b03464
ACS Sustainable Chem. Eng. 2018, 6, 2047−2054

usually results in low loading and weak bonding between biomolecules and the PLA scaffold. Fortunately, surface modification with dopamine has already become an efficient and feasible method to endow biological functionality on various materials.[14] Blending with hydroxyapatites (HAs) has been applied for better cell compatibility, osteoconductivity, and osteoinductivity because it is a major inorganic component of the bone.[15,16] Needlelike nanohydroxyapatite (nHA) possesses a high surface area to volume ratio; thus, a small amount may be sufficient for the enhancement of bioactivity and osseointegration.[17] Dopamine coating made the blending of gelatin with nHA available for necessary nutrient supply, but effective antibacterial activity for the in vivo scaffold could not be ignored as well.[18] Besides osteostimulation and angiogenesis, there is a growing clinical need for antimicrobial devices, as antibiotics are no longer an ideal solution due to challenges in reaching the target organisms, especially when associated with a medical device.[19] Therefore, after modification with dopamine, ponericin G1, which was isolated from the venom of the ponerine ant *P. goeldii*, was also grafted onto the surface to endow the scaffold with excellent antibacterial properties because ponericin G is first considered as cecropin-like members, which have a broad spectrum of activity against bacteria and fungi but do not affect most other eukaryotic cells.[20−22] To the best of our knowledge, this is the first ponericin-incorporating scaffold for bone tissue regeneration, and it is expected to be an efficient implant for in vivo application.

EXPERIMENTAL SECTION

Materials. PLA filament (M_n = 15 kDa) was supplied by Zhejiang Hisun Pharmaceutical Co., Ltd. Gelatin was offered by Sigma-Aldrich. The grade of chemicals was analytical grade or higher. nHA powder was obtained from Beijing DK nano technology Co., Ltd. Ponericin G1 peptide was purchased from Top-peptide Co., Ltd.

Preparation of 3D-Printed Scaffold. 3D-printed scaffolds were designed using Solid work software, and the model was converted into an stl file, which was a standard software interface for rapid manufacturing devices. The 3D printing machine Creality 3D CR-8S was employed to fabricate the porous scaffolds. The maximum build volume was 21 × 21 × 21 cm^3, and the diameter of the extrusion nozzle was 0.4 mm. The thickness of each layer was designed to be 0.1 mm, and the pinpoint scanning speed was set to be 30 mm/s to acquire higher accuracy. During the printing process, the PLA filament was drawn and melted at ∼220 °C followed by extrusion through the print tip to deposit a layer of beads adhering onto the bed (bed temperature is set to be 60 °C, and the room temperature is maintained at 25 °C) and processed in diameter 0.5 mm, gap 0.5 mm. A mesh structure (a 0°/90° strut structure) was obtained using a layer-by-layer manner.

Porosity. The theoretical porosity percentage (%$Vol_{theoretical}$) was calculated from each scaffold's geometry using the initially designed parameters. Porosity was calculated by means of the equation

$$\%Vol_{theoretical} = (1 - (\Phi^2/4)\pi N_c N_l/(wh))100\% \quad (1)$$

where Φ, w, and h refer to the strut diameter, scaffold width, and scaffold height, respectively. Furthermore, N_c represents the number of struts per layer, and N_l represents the number of layers per scaffold. No overlap between struts was considered.[23,24]

Mechanical Tests. Mechanical tests were performed on cubic specimens (10 mm × 10 mm × 10 mm). The cross-head speed during loading in the universal testing machine (Instron 1121, UK) was 5 mm/min. Three specimens were tested for mean value calculations.

Dopamine Modification and Coating of the PLA Scaffold with Gelatin/nHA/Ponericin. The deposition of dopamine onto the PLA scaffold was conducted via direct immersion coating. All the materials were rinsed with deionized water before immersion. For the polymerization of dopamine into polydopamine, the substrates were immersed into a dopamine solution (2 mg/mL in 10 mM Tris, pH 8.5) at room temperature for 12 h followed by several rinses with deionized water. Then, the scaffold was immersed into the gelatin/nHA/ponericin solution to be endowed with multiple functions.

Characterization of the Coating. The surface chemical compositions of the specimens were measured by X-ray photoelectron spectroscopy (XPS, Al Kα, Thermo Electron, USA). The microstructure of scaffolds was examined under a scanning electron microscope (SEM, Philips XL30). Water contact angle measurements were performed to evaluate the material's wettability by randomly putting 3 drops of 2 μL of milliQ water with a syringe onto the surfaces, and the image was taken by a CCD camera (VCA 2000, AST).

MC3T3-E1 Cell Culture and Cell Morphology. Mouse preosteoblastic MC3T3-E1 cells were cultured in the DMEM culture medium consisting of 10% fetal bovine serum (FBS) and 1% penicillin/streptomycin and kept in a humidified atmosphere with 5% CO_2 at 37 °C.

After seeding 1 × 10^5 cells for each scaffold and incubation for 24 h, cells on the scaffold were fixed with 4% paraformaldehyde (PFA) in phosphate-buffered saline (PBS) for 15 min followed by rinsing with PBS. Subsequently, it was incubated with fluorescein isothiocyanate (FITC, 1 mg/mL in DMSO) for 7 min and rinsed with PBS for three times. Afterward, the nuclei were stained with 4′,6-diamidino-2-phenylindole, dilactate (DMSO) for 5 min at room temperature. Repeated rinsing with PBS was also conducted, and cell adhesion and migration on the substrate were viewed with a confocal laser scanning microscope (CLSM).

dLive/Dead Staining. MC3T3-E1 cells (1 × 10^5 cells per well) were seeded onto each scaffold placed in a 12-well plate and cultured for 72 h. Afterward, a Live−Dead assay kit was employed to gain a qualitative viability assay. At the predesigned time, these scaffolds containing cells were washed with PBS three times and treated with calcein AM (2 μM) and propidium iodide (4 μM) for 30 min at room temperature according to the illustration. Cells were observed under an inverted fluorescence microscope (TE2000U, Nikon).

Cell Proliferation Assays. Cell suspensions at densities of 5 × 10^4 and 3 × 10^4 cells/mL were seeded on different scaffolds placed in the 96-well plates. At 24 and 72 h, WST-8 solution (10% v/v in medium) (Cell Counting Kit-8) was added to each well. After 2 h of incubation, 100 μL of each well was removed to a new 96-well plate; the absorbance value at 450 nm was measured on a multifunction microplate scanner (Tecan Infinite M 200), and the relative cell proliferation rate was calculated.

Osteogenesis Assay. The level of alkaline phosphatase (ALP) activity was determined by quantitation of the enzyme activity after cell seeding for 7 and 14 days as described in the literature.[25,26] After removal of the medium, MC3T3-E1 cells were washed with PBS, lysed with RIPA buffer, and split by repeated freeze and thawing. Then, *p*-nitrophenol phosphate substrate (pNPP) solution was added and incubated in the dark at 37 °C for 30 min. The spectrophotometric values at 405 nm were determined via a full wavelength reader. All experiments were performed in triplicate.

Cell Differentiation Assays. Calcium deposition was assessed with Alizarin Red-S (ARS) staining of MC3T3-E1 cells after incubation on all scaffolds for 21 days. The scaffolds with attached cells were washed three times with PBS (pH 7.4) and fixed with 4% glutaraldehyde solution for 15 min. After washing three times again with phosphate buffer, the scaffolds were subjected to 1% ARS solution (pH 4.2 in Tris) for 30 min at 37 °C. Subsequently, the excess dye was gently washed off, and photographs were captured by the microscope.

Antibacterial Study. For the antibacterial effect of various scaffolds to be investigated, the scaffolds were mixed with 3 mL of *Staphylococcus aureus* (*S. aureus*) and *Escherichia coli* (*E. coli*) in LB culture medium (4.0 × 10^4 bacteria/mL), respectively, and cultured for 18 and 24 h. Aliquots of 0.1 mL from each group were transferred to a new 96-well plate. Plates were read in a multiwell

DOI: 10.1021/acssuschemeng.7b03464
ACS Sustainable Chem. Eng. 2018, 6, 2047−2054

Scheme 1. Schematic Illustration of a Composite 3D-Printed PLA Scaffold for Bone Regeneration

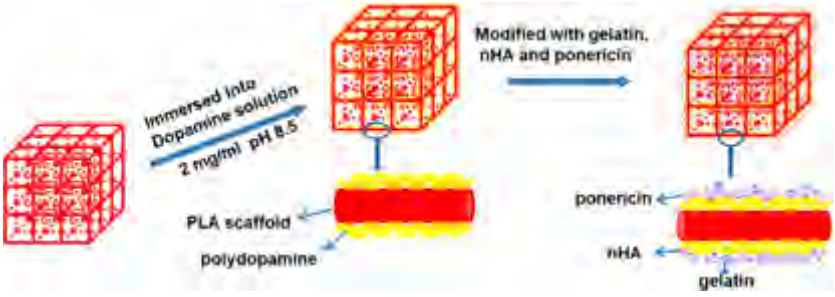

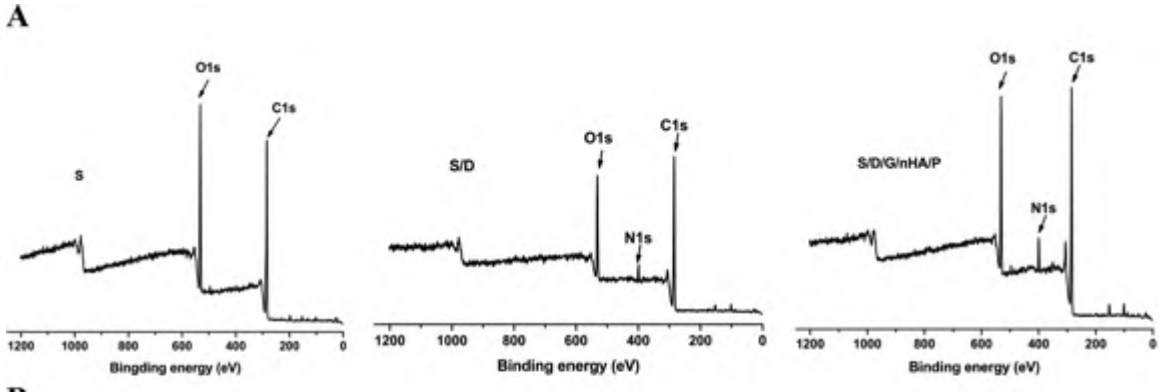

B

	C	N	O
S	73.26	1.01	25.73
S/D	76.41	4.94	18.65
S/D/G/nHA/P	73.21	5.18	21.61

Figure 1. XPS spectra (A) and surface chemical composition (B) of untreated PLA scaffold (S), dopamine-modified scaffold (S/D), and ponericin-incorporating scaffold (S/D/G/nHA/P).

spectrophotometer at OD 600 nm, and the results were obtained in triplicate.

Approximately 10^5 CFU of *S. aureus* and *E. coli* were first plated on nutrient agar separately, and the samples were cut into small disks and laid for 24 h at 37 °C.

RESULTS AND DISCUSSION

The combination of the modern manufacturing techniques (including 3D printing) and imaging techniques, such as computed tomography (CT) and magnetic resonance imaging (MRI), made the fabrication of a customized scaffold, which was precisely shaped to satisfy the unique patient anatomy and defect location, possible.[27] It has also been realized that definite micro architecture and porosity including pore size, its distribution and connectivity in 3D scaffolds play a crucial role in recreating a tissue-like cell mass.[28,29] Herein, with the aid of Solid work software, we printed a programmed interlined PLA scaffold with a calculated porosity of 67% (according to eq 1) similar to the inner cancellous bone, which is spongy in nature, having 50−90 vol % porosity.[30] Although higher porosity is more beneficial for blood vessel ingrowth, oxygen delivery, and nutrient and waste diffusion, the accompanied loss of mechanical characteristics must be taken into consideration.[4,31] As expected, the increase in scaffold porosity diminished the compressive strength from the initial 90.1 MPa (0% porosity) to 3.3 MPa (67% porosity), but the porous scaffold was still available to provide resistance to temporary load in the restoring period.

At alkaline pH and in the presence of atmospheric oxygen, dopamine is slowly auto-oxidized to create an adhesive polydopamine layer on various material surfaces.[14] Although uniformly distributed multilayer Ag nanoparticles (SNPs) could be generated through alternative dipping the film in dopamine and silver nitrate solution, and the multilayered SNPs demonstrated a significant enhancement in antibacterial and catalytic performance,[32] the human immune system was the most sensitive parameter to the side effects rendered by nanosilver, particularly at high concentrations.[33] Because of their small size and high mobility, Ag NPs could enter mammalian cells and cause mitochondrial damage, inducing apoptosis and cell death.[34,35] On the other hand, ponericin G1 has biocidal activity against a broad spectrum of bacteria and gunji, and it could be synthesized manually without any immunological concern.[20] As illustrated in Scheme 1, first of all, the 3D-printed scaffold was immersed into an alkaline solution of dopamine for 12 h to form an adherent polydopamine coating. Subsequently, the modified scaffold was used as supports to immobilize the mixture of gelatin, nHA, and ponericin because the polydopamine surface also held active quinone groups that could form Michael addition and/or Schiff base with gelatin and ponericin, which contained primary amine and thiol groups.[36,37]

DOI: 10.1021/acssuschemeng.7b03464
ACS Sustainable Chem. Eng. 2018, 6, 2047−2054

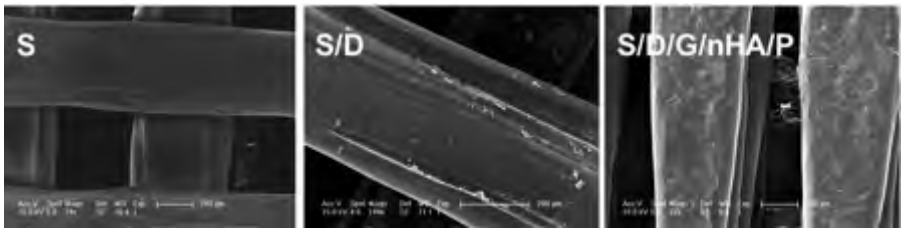

Figure 2. Scanning electron micrographs (SEM) of PLA scaffold (S), dopamine-modified scaffold (S/D), and ponericin-immobilized scaffold (S/D/G/nHA/P).

Successful surface modification of the fabricated scaffold using dopamine chemistry was confirmed by XPS (Figure 1A). The photoelectron peaks of the polydopamine coating appeared along with emergence of N 1s and C 1s at 400 and 285 eV, which was in accordance with the literature.[38] After polydopamine coating, the carbon and nitrogen contents became greater than those of the untreated PLA scaffold. An obvious increase of N 1s, from 1.01 to 4.94% for the polydopamine coating scaffold, was also observed, confirming the polymerization and deposition of dopamine on the substrate. Moreover, as shown in Figure 1B, a further increase of N content was caused by the grafting of gelatin/nHA/ponericin on the scaffold.

SEM analysis was conducted to scan the morphology and microstructures of the 3D-printed PLA scaffold. As presented in Figure 2, the image showed that the diameters of the scaffolds were 0.5 mm, and highly connected porosity could also be observed, which was in accordance with the design. Before immersion in dopamine, the surface of PLA scaffolds was smooth, and the shape was uniform. After dopamine polymerization, lumps of coated polydopamine were observed on the surface of the scaffold, which was consistent with previous reports, and the results indicated that the polydopamine coating did not change the surface morphology to a large extent.[39] Ideal rougher morphology was gained only after the following gelatin/nHA/ponericin G1 grafting, where the newly formed nanostructures spread homogeneously all over the surfaces and they were quite desirable for cell anchoring, adhesion, and proliferation.[40]

Wettability of different scaffolds was evaluated using the water contact angle assay (Figure 3). The untreated PLA scaffold showed a contact angle of 74.9°, which exhibited hydrophobic properties and was not beneficial for cell culture.[41] After polydopamine coating, the water drop was immediately absorbed, and the surface became totally hydrophilic and showed a drastic decrease in the water contact angle to 0°, which could be varied with different coating times, concentrations of dopamine solution, and reaction temperatures.[39,42,43] However, after gelatin/ponericin G1 modification, a notably different phenomenon was observed. The contact angle exhibited a gradual decrease from 81.8° to a final value of 21.2° in 1.5 min. This could be the contribution of nHA because scaffolds modified with dopamine and gelatin showed a constant value of the water contact angle, whereas modification with nHA together caused the coating defects due to the poor interfacial properties and phase separation between gelatin and nHA. Therefore, the water drop gradually came into contact with naked dopamine and led to a decrease in the value.

For the effects of polydopamine and gelatin/nHA/ponericin modifications on MC3T3-E1 cell adhesion and proliferation to

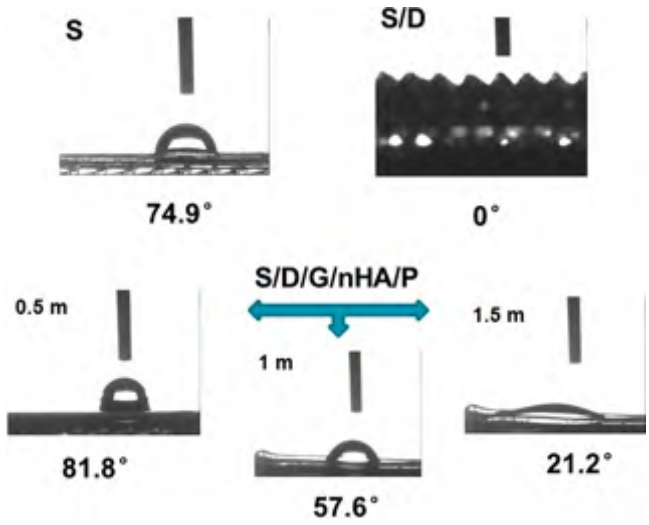

Figure 3. Wettability assessment of different scaffolds by water contact angle detection.

be investigated, CLSM was first conducted after 24 h cell culture (Figure 4). It could be seen that cells mostly adhered along the edge of the scaffold for the untreated PLA substrate and adopted a rounded shape. Dopamine modification significantly promoted cell adhesion. After further coating with gelatin/nHA/ponericin, the quantity of cell attachment seemed to decrease compared with that of the dopamine-modified scaffold, but the distribution was uniform all over the surface. At the same time, cells still spread out more than on the naked PLA scaffold and maintained a relatively healthy morphology. Further live/dead staining confirmed that, after 3 days culture, cells on the scaffolds were all in a good state of living, indicating that dopamine-coated and gelatin/nHA/ponericin-modified scaffolds could be suitable carriers for living cell adhesion (Figure 5).

As shown in the CCK-8 analysis (Figure 6), after 24 h culture, dopamine deposition showed an increased cell proliferation compared with that of other scaffold groups. The possible reason could be ascribed mainly to three cues: (1) extremely hydrophilic surface beneficial for improving cell attachment, (2) bioactive functional groups such as OH and NH_2, and (3) immobilization of serum proteins that could not only react with polydoppamine but also maintain their native activity and thus serve as cell adhesion sites.[44−46] We conclude that (1) and (3) predominated cell adhesion at the earlier stage because gelatin and nHA also held sufficient bioactive groups. On the other hand, with the exhaustion of serum, this obvious predominance in the quantities of cell proliferation on the polydopamine-coated scaffold disappeared after 3 days of culture because gelatin and nHA also supported the cell

DOI: 10.1021/acssuschemeng.7b03464
ACS Sustainable Chem. Eng. 2018, 6, 2047−2054

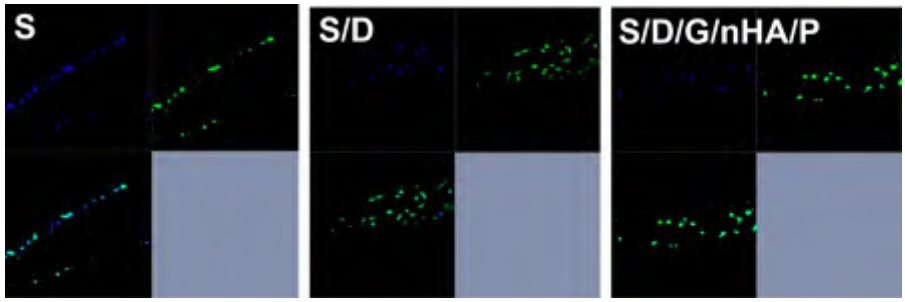

Figure 4. Morphology and adhesion of MC3T3-E1 cells on various scaffolds investigated by CLSM.

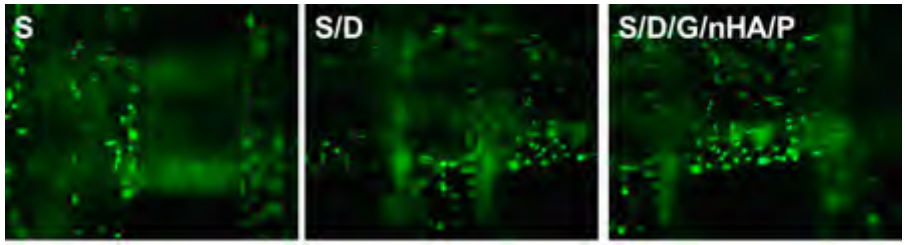

Figure 5. Live/dead staining images of MC3T3-E1 cells cultured on different scaffolds.

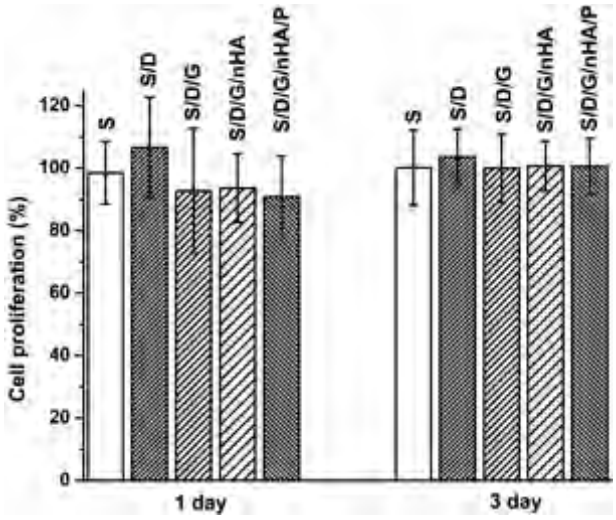

Figure 6. Evaluation of MC3T3-E1 cell proliferation on S, S/D, and S/D/G/nHA/P for 1 and 3 d by CCK-8 analysis.

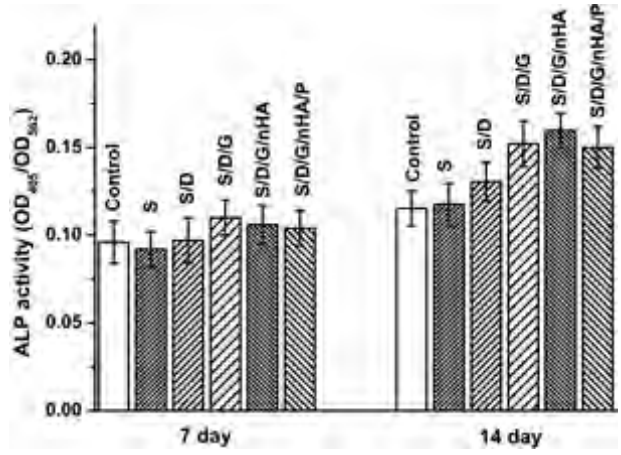

Figure 7. Alkaline phosphatase activity of MC3T3-E1 cells on different scaffolds after 7 and 14 d of culture.

adhesion and proliferation.[47,48] Furthermore, ponericin did not show a cell killing effect toward MC3T3-E1 cells during this procedure.

ALP enzyme activity, an indicator of osteoconductivity, is one of the main conventional markers of osteoblastic phenotype expression and is usually associated with bone formation at high levels.[7] The ALP expression of MC3T3-E1 cultured on different substrates after 7 and 14 days has also been examined (Figure 7). Higher ALP secretions were observed on gelatin-immobilized scaffolds. After 7 days of culture, S/D/G showed the most ALP secretion with a value of 11.02%, and the other two groups of S/D/G/nHA and S/D/G/nHA/P showed values of 10.61 and 10.42%, respectively. This predominance of gelatin-incorporating scaffolds was more obvious after 14 days of culture, and nHA was also beneficial for the increase in ALP activity.[7] These results confirmed our earlier supposition that gelatin and nHA began to take effect at the later stage instead of serum and that ponericin did not down shift the secretion of ALP in comparison with that of the S/D/G/nHA scaffold.

ARS staining was conducted to visualize the accumulated calcium deposition, as shown in Figure 8. Some mineral depositions were observed on the edge of the bare PLA scaffold after culture for 3 weeks. In the presence of dopamine, a bone nodule was uniformly distributed all over the strut. Notably, an intense calcium staining was exhibited on the S/D/G/nHA/P group, and newly formed interconnected cells were generated between adjacent columns. The results confirmed that the S/D/G/nHA/P scaffold induced more satisfactory mineralization because of the composite structure, confirming its ability to improve bone growth.

Both *E. coli* and *S. aureus* were investigated in our experiments. When the concentration of ponericin solution was controlled at 250 μg/mL, the antibacterial activity did not vary with the increase in concentration of gelatin, indicating that the incorporating ponericin amount had nothing to do with viscosity of the immersion solution (data not shown). However, when the concentration of gelatin was controlled at

DOI: 10.1021/acssuschemeng.7b03464
ACS Sustainable Chem. Eng. 2018, 6, 2047−2054

Figure 8. Calcium deposition evaluated by AlizarinRed S staining of MC3T3-E1 cells cultured on PLA scaffold (S), dopamine-modified scaffold (S/D), and hybrid scaffold (S/D/G/nHA/P) after 14 d of culture.

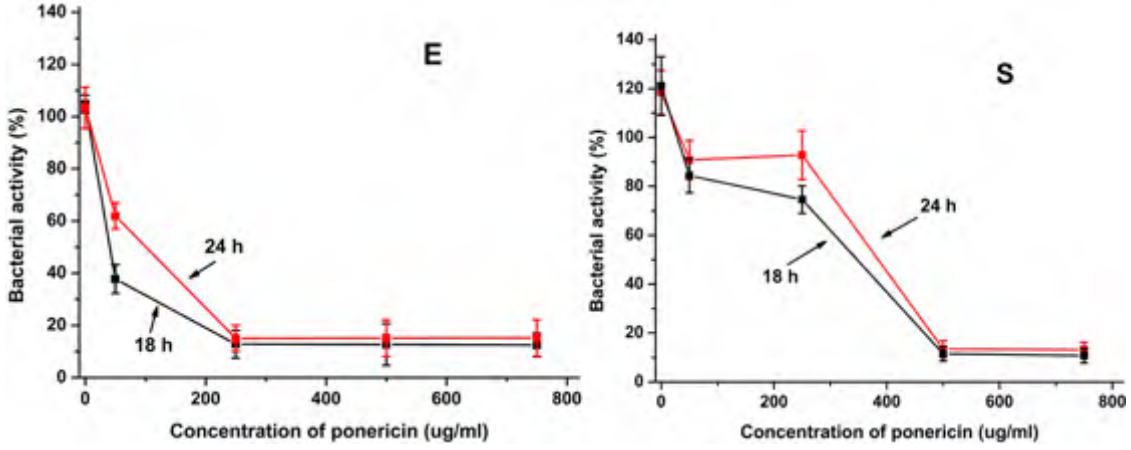

Figure 9. Antibacterial effect of the ponericin-modified scaffold (S/D/G/nHA/P) against *E. coli* (E) and *S. aureus* (S) at different concentrations of ponericin solution.

3%, the OD value of the bacteria culture varied to a large extent in proportion with the concentration of ponericin solution (ranging from 50 to 750 μg/mL), as shown in Figure 9. For *E. coli*, the best antibacterial effect was achieved at 250 μg/mL, whereas for *S. aureus*, the value increased to 500 μg/mL. After 24 h of culture, the same trend was obtained for both *E. coli* and *S. aureus* as 18 h, and the relative percentage was still satisfied with only a little decrease in the antibacterial activity. It could be concluded that the ponericin-incorporating scaffold was more sensitive to *E. coli* than *S. aureus* and that the scaffold was able to maintain long-term antibacterial activity. As shown in Figure 10, an obvious inhibition zone was observed for both *E. coli* and *S. aureus* after 24 h of culture on nutrient agar. In fact, the inhibition zone was still quite clear until 72 h. On the other hand, results of SEM (Figure 11) also proved that both the Gram-positive and -negative bacteria adhered on the scaffold shrunk to spheres with a diameter of 1 μm, indicating that the antibacterial activity was maintained in the prepared scaffold and would be applied as an excellent antibacterial implant.

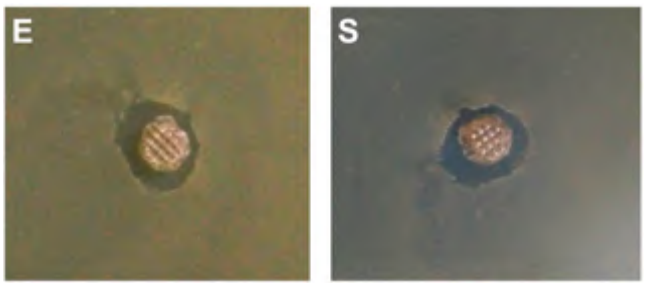

Figure 10. Inhibition zones study of the hybrid scaffold (S/D/G/nHA/P) against *E. coli* (E) and *S. aureus* (S) after 12 h of culture at 37 °C.

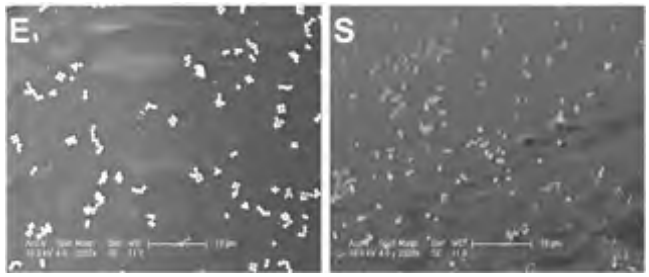

Figure 11. SEM images of *E. coli* (E) and *S. aureus* (S) grown on S/D/G/nHA/P after 18 h of culture.

CONCLUSIONS

3D-printed PLA scaffold was prepared through the FDM method. With high interconnectivity and porosity, the scaffolds enabled MC3T3-E1 cells to adhere, proliferate, and calcite through both the outer and inner parts. Polydopamine modification made the scaffold totally hydrophilic and have more affinity to serum, which thus caused an early increase in cell proliferation, but the gelatin-containing group began to take effect at a later ALP section and the S/D/G/nHA/P group improved calcium deposition. Antibacterial experiments confirmed that the activity of ponericin was well kept in the S/D/G/nHA/P scaffold and was more sensitive toward *E. coli* than *S. aureus*. All the results presented above prove that this composite 3D-printed scaffold could simultaneously enhance

DOI: 10.1021/acssuschemeng.7b03464
ACS Sustainable Chem. Eng. 2018, 6, 2047−2054

the osteogenicity of MC3T3-E1 cells and be utilized as an in situ antibacterial agent.

AUTHOR INFORMATION

Corresponding Authors

*E-mail: ybhuang@ciac.ac.cn.
*E-mail: zhangpb@Gmail.com.

ORCID

Xuesi Chen: 0000-0003-3542-9256
Yubin Huang: 0000-0002-5212-318X

Notes

The authors declare no competing financial interest.

ACKNOWLEDGMENTS

The authors are thankful for financial support from National Natural Science Foundation of China (Nos. 311421001, 711491001, and 211201001).

ABBREVIATIONS

S	neat PLA scaffold
S/D	dopamine-modified scaffold
S/D/G	gelatin-added scaffold
S/D/G/nHA	nHA- and gelatin-containing scaffold
S/D/G/nHA/P	ponericin-added scaffold.

REFERENCES

(1) Farokhi, M.; Mottaghitalab, F.; Shokrgozar, M. A.; Ou, K. L.; Mao, C.; Hosseinkhani, H. Importance of dual delivery systems for bone tissue engineering. *J. Controlled Release* **2016**, *225*, 152−169.

(2) Fernandez-Yague, M. A.; Abbah, S. A.; McNamara, L.; Zeugolis, D. I.; Pandit, A.; Biggs, M. J. Biomimetic approaches in bone tissue engineering: integrating biological and physicomechanical strategies. *Adv. Drug Delivery Rev.* **2015**, *84*, 1−29.

(3) Shin, H.; Jo, S.; Mikos, A. G. Biomimetic materials for tissue engineering. *Biomaterials* **2003**, *24* (24), 4353−4364.

(4) Ceccarelli, G.; Presta, R.; Benedetti, L.; Cusella De Angelis, M. G.; Lupi, S. M.; Rodriguez, Y. B. R. Emerging perspectives in scaffold for tissue engineering in oral surgery. *Stem Cells Int.* **2017**, *10*, 1.

(5) Evans, N. D.; Gentleman, E.; Polak, J. M. Scaffolds for stem cells. *Mater. Today* **2006**, *9* (12), 26−33.

(6) Kucharska, M.; Butruk, B.; Walenko, K.; Brynk, T.; Ciach, T. Fabrication of in-situ foamed chitosan/β-TCP scaffolds for bone tissue engineering application. *Mater. Lett.* **2012**, *85*, 124−127.

(7) Fayyazbakhsh, F.; Solati-Hashjin, M.; Keshtkar, A.; Shokrgozar, M. A.; Dehghan, M. M.; Larijani, B. Novel layered double hydroxides-hydroxyapatite/gelatin bone tissue engineering scaffolds: fabrication, characterization, and in vivo study. *Mater. Sci. Eng., C* **2017**, *76*, 701−714.

(8) Cao, H.; Kuboyama, N. A biodegradable porous composite scaffold of PGA/β-TCP for bone tissue engineering. *Bone* **2010**, *46* (2), 386−395.

(9) Cui, L.; Zhang, N.; Cui, W.; Zhang, P.; Chen, X. A novel nano/micro-fibrous scaffold by melt-spinning method for bone tissue engineering. *J. Bionic Eng.* **2015**, *12* (1), 117−128.

(10) Sanatgar, R. H.; Campagne, C.; Nierstrasz, V. Investigation of the adhesion properties of direct 3D printing of polymers and nanocomposites on textiles: effect of FDM printing process parameters. *Appl. Surf. Sci.* **2017**, *403*, 551−563.

(11) Pedde, R. D.; Mirani, B.; Navaei, A.; Styan, T.; Wong, S.; Mehrali, M.; Thakur, A.; Mohtaram, N. K.; Bayati, A.; Dolatshahi-Pirouz, A.; Nikkhah, M.; Willerth, S. M.; Akbari, M. Emerging biofabrication strategies for engineering complex tissue constructs. *Adv. Mater.* **2017**, *29* (19), 1606061.

(12) Bogue, R. 3D printing: the dawn of a new era in manufacturing? *Assembly Autom.* **2013**, *33* (4), 307−311.

(13) Malinauskas, M.; Rekštytė, S.; Lukoševičius, L.; Butkus, S.; Balčiūnas, E.; Pečiukaitytė, M.; Baltriukienė, D.; Bukelskienė, V.; Butkevičius, A.; Kucevičius, P. 3D microporous scaffolds manufactured via combination of fused filament fabrication and direct laser writing ablation. *Micromachines* **2014**, *5* (4), 839−858.

(14) Lee, H.; Dellatore, S. M.; Miller, W. M.; Messersmith, P. B. Mussel-inspired surface chemistry for multifunctional coatings. *Science* **2007**, *318* (5849), 426−430.

(15) Hong, Z.; Zhang, P.; He, C.; Qiu, X.; Liu, A.; Chen, L.; Chen, X.; Jing, X. Nano-composite of poly(L-lactide) and surface grafted hydroxyapatite: mechanical properties and biocompatibility. *Biomaterials* **2005**, *26* (32), 6296−6304.

(16) Kumar, P. T.; Srinivasan, S.; Lakshmanan, V. K.; Tamura, H.; Nair, S. V.; Jayakumar, R. Synthesis, characterization and cytocompatibility studies of α-chitin hydrogel/nano hydroxyapatite composite scaffolds. *Int. J. Biol. Macromol.* **2011**, *49* (1), 20−31.

(17) Chen, F.; Wang, Z. C.; Lin, C. J. Preparation and characterization of nano-sized hydroxyapatite particles and hydroxyapatite/chitosan nano-composite for use in biomedical materials. *Mater. Lett.* **2002**, *57* (4), 858−861.

(18) Chien, C. Y.; Liu, T. Y.; Kuo, W. H.; Wang, M. J.; Tsai, W. B. Dopamine-assisted immobilization of hydroxyapatite nanoparticles and RGD peptides to improve the osteoconductivity of titanium. *J. Biomed. Mater. Res., Part A* **2013**, *101* (3), 740−747.

(19) Fernandes, J. S.; Gentile, P.; Pires, R. A.; Reis, R. L.; Hatton, P. V. Multifunctional bioactive glass and glass-ceramic biomaterials with antibacterial properties for repair and regeneration of bone tissue. *Acta Biomater.* **2017**, *59*, 2−11.

(20) Orivel, J.; Redeker, V.; Le Caer, J. P.; Krier, F.; Revol-Junelles, A. M.; Longeon, A.; Chaffotte, A.; Dejean, A.; Rossier, J. Ponericins, New antibacterial and insecticidal peptides from the venom of the ant Pachycondyla goeldii. *J. Biol. Chem.* **2001**, *276* (21), 17823−17829.

(21) Boman, H. G.; Dan, H. Cell-free immunity in insects. *Trends Biochem. Sci.* **1981**, *6* (41), 306−309.

(22) Ekengren, S.; Hultmark, D. Drosophila cecropin as an antifungal agent. *Insect Biochem. Mol. Biol.* **1999**, *29* (11), 965−972.

(23) Serra, T.; Planell, J. A.; Navarro, M. High-resolution PLA-based composite scaffolds via 3-D printing technology. *Acta Biomater.* **2013**, *9* (3), 5521−5530.

(24) Serra, T.; Ortiz-Hernandez, M.; Engel, E.; Planell, J. A.; Navarro, M. Relevance of PEG in PLA-based blends for tissue engineering 3D-printed scaffolds. *Mater. Sci. Eng., C* **2014**, *38*, 55−62.

(25) Wang, Z.; Chen, L.; Wang, Y.; Chen, X.; Zhang, P. Improved cell adhesion and osteogenesis of op-HA/PLGA composite by poly(dopamine)-assisted immobilization of collagen mimetic peptide and osteogenic growth peptide. *ACS Appl. Mater. Interfaces* **2016**, *8* (40), 26559−26569.

(26) Tsai, W. B.; Chen, P. Y.; Wei, K. L.; Chen, Y. R.; Liao, T. Y.; Liu, H. L.; Lai, J. Y. Polyelectrolyte multilayer films functionalized with peptides for promoting osteoblast functions. *Acta Biomater.* **2009**, *5* (9), 3467−3477.

(27) Forrestal, D. P.; Klein, T. J.; Woodruff, M. A. Challenges in engineering large customized bone constructs. *Biotechnol. Bioeng.* **2017**, *114* (6), 1129−1139.

(28) Agarwal, T.; Kabiraj, P.; Narayana, G. H.; Kulanthaivel, S.; Kasiviswanathan, U.; Pal, K.; Giri, S.; Maiti, T. K.; Banerjee, I. Alginate bead based hexagonal close packed 3D implant for bone tissue engineering. *ACS Appl. Mater. Interfaces* **2016**, *8* (47), 32132−32145.

(29) Dutta, R. C.; Dey, M.; Dutta, A. K.; Basu, B. Competent processing techniques for scaffolds in tissue engineering. *Biotechnol. Adv.* **2017**, *35* (2), 240−250.

(30) Bose, S.; Vahabzadeh, S.; Bandyopadhyay, A. Bone tissue engineering using 3D printing. *Mater. Today* **2013**, *16* (12), 496−504.

(31) Polocorrales, L.; Latorreesteves, M.; Ramirezvick, J. E. Scaffold design for bone regeneration. *J. Nanosci. Nanotechnol.* **2014**, *14* (1), 15−56.

DOI: 10.1021/acssuschemeng.7b03464
ACS Sustainable Chem. Eng. 2018, 6, 2047−2054

(32) Sureshkumar, M.; Lee, P. N.; Lee, C. K. Stepwise assembly of multimetallic nanoparticles via self-polymerized polydopamine. *J. Mater. Chem.* **2011**, *21* (33), 12316−12320.
(33) De Jong, W. H.; Van Der Ven, L. T.; Sleijffers, A.; Park, M. V.; Jansen, E. H.; Loveren, H. V.; Vandebriel, R. J. Systemic and immunotoxicity of silver nanoparticles in an intravenous 28 days repeated dose toxicity study in rats. *Biomaterials* **2013**, *34* (33), 8333−8343.
(34) Singh, R. P.; Ramarao, P. Cellular uptake, intracellular trafficking and cytotoxicity of silver nanoparticles. *Toxicol. Lett.* **2012**, *213* (2), 249−259.
(35) Roubelakis, M. G.; Bitsika, V.; Zagoura, D.; Trohatou, O.; Pappa, K. I.; Makridakis, M.; Antsaklis, A.; Vlahou, A.; Anagnou, N. P. In vitro and in vivo properties of distinct populations of amniotic fluid mesenchymal progenitor cells. *J. Cell. Mol. Med.* **2011**, *15* (9), 1896−1913.
(36) Lee, H.; Rho, J.; Messersmith, P. B. Facile conjugation of biomolecules onto surfaces via mussel adhesive protein inspired coatings. *Adv. Mater.* **2009**, *21* (4), 431−434.
(37) Chao, C.; Liu, J.; Wang, J.; Zhang, Y.; Zhang, B.; Zhang, Y.; Xiang, X.; Chen, R. Surface modification of halloysite nanotubes with dopamine for enzyme immobilization. *ACS Appl. Mater. Interfaces* **2013**, *5* (21), 10559−10564.
(38) Yang, Y.; Qi, P.; Wen, F.; Li, X.; Xia, Q.; Maitz, M. F.; Yang, Z.; Shen, R.; Tu, Q.; Huang, N. Mussel-inspired one-step adherent coating rich in amine groups for covalent immobilization of heparin: hemocompatibility, growth behaviors of vascular cells, and tissue response. *ACS Appl. Mater. Interfaces* **2014**, *6* (16), 14608−14620.
(39) Rim, N. G.; Kim, S. J.; Shin, Y. M.; Jun, I.; Lim, D. W.; Park, J. H.; Shin, H. Mussel-inspired surface modification of poly(l-lactide) electrospun fibers for modulation of osteogenic differentiation of human mesenchymal stem cells. *Colloids Surf., B* **2012**, *91*, 189−197.
(40) Shekaran, A.; García, A. J. Extracellular matrix-mimetic adhesive biomaterials for bone repair. *J. Biomed. Mater. Res., Part A* **2015**, *96A* (1), 261−272.
(41) He, W.; Ma, Z.; Yong, T.; Teo, W. E.; Ramakrishna, S. Fabrication of collagen-coated biodegradable polymer nanofiber mesh and its potential for endothelial cells growth. *Biomaterials* **2005**, *26* (36), 7606−7615.
(42) Kao, C. T.; Lin, C. C.; Chen, Y. W.; Yeh, C. H.; Fang, H. Y.; Shie, M. Y. Poly(dopamine) coating of 3D printed poly(lactic acid) scaffolds for bone tissue engineering. *Mater. Sci. Eng., C* **2015**, *56*, 165−173.
(43) Wu, C.; Han, P.; Liu, X.; Xu, M.; Tian, T.; Chang, J.; Xiao, Y. Mussel-inspired bioceramics with self-assembled Ca-P/polydopamine composite nanolayer: preparation, formation mechanism, improved cellular bioactivity and osteogenic differentiation of bone marrow stromal cells. *Acta Biomater.* **2014**, *10* (1), 428−438.
(44) Ku, S. H.; Park, C. B. Human endothelial cell growth on mussel-inspired nanofiber scaffold for vascular tissue engineering. *Biomaterials* **2010**, *31* (36), 9431−9437.
(45) Wu, C.; Fan, W.; Chang, J.; Xiao, Y. Mussel-inspired porous SiO_2 scaffolds with improved mineralization and cytocompatibility for drug delivery and bone tissue engineering. *J. Mater. Chem.* **2011**, *21* (45), 18300−18307.
(46) Wang, M.; Favi, P.; Cheng, X.; Golshan, N. H.; Ziemer, K. S.; Keidar, M.; Webster, T. J. Cold atmospheric plasma (CAP) surface nanomodified 3D printed polylactic acid (PLA) scaffolds for bone regeneration. *Acta Biomater.* **2016**, *46*, 256−265.
(47) Qu, T.; Liu, X. Nano-structured gelatin/bioactive glass hybrid scaffolds for the enhancement of odontogenic differentiation of human dental pulp stem cells. *J. Mater. Chem. B* **2013**, *1* (37), 4764−4772.
(48) Thomson, R. C.; Yaszemski, M. J.; Powers, J. M.; Mikos, A. G. Hydroxyapatite fiber reinforced poly(α-hydroxy ester) foams for bone regeneration. *Biomaterials* **1998**, *19* (21), 1935−1943.

DOI: 10.1021/acssuschemeng.7b03464
ACS Sustainable Chem. Eng. 2018, 6, 2047−2054